

Article

Optical Limiting from CdSe-Based Multiphase Polymer Nanocomposite Films

Leah M. Eversole, Richard Adjorlolo, Jack Francis Renaud and Mithun Bhowmick * 

Department of Mathematical and Physical Sciences, Miami University Regionals, Middletown, OH 45042, USA; eversolm@miamioh.edu (L.M.E.); adjorlr@miamioh.edu (R.A.); renaudjf@miamioh.edu (J.F.R.)

* Correspondence: bhowmim@miamioh.edu

Abstract: Closely packed nanoparticles in polymer films are interesting materials where collective as interactive optical properties could be tuned based on nanoparticle proximity, surface morphology, types of encapsulation and matrix parameters. Two types of polymers (polymethylmethacrylate (PMMA) and polyvinyl alcohol (PVA))-based nanocomposite films featuring dual-colored emission peaks (~578 nm and ~650 nm) were fabricated from CdSe quantum dots to study their viability in optoelectronic applications. Using a 405 nm excitation laser, the evolution of photoluminescence (PL) intensities and peak wavelengths were examined as a function of increasing excitation intensity. While PL intensities showed systematic saturation and quenching, the emission wavelengths were found to be linearly red shifting with increasing excitation intensities in the PMMA films. The 650 nm emitting QDs seem to tune the PL saturation behavior in these films, as opposed to the PVA-based materials, where no such impact was seen. The material system could be a low-cost, low-maintenance alternative for future mesoscale sensing and light-emitting device applications.

Keywords: quantum dots; polymethyl methacrylate; polyvinyl alcohol; photoluminescence; polymer nanocomposites; CdSe



Citation: Eversole, L.M.; Adjorlolo, R.; Renaud, J.F.; Bhowmick, M. Optical Limiting from CdSe-Based Multiphase Polymer Nanocomposite Films. *Coatings* **2024**, *14*, 634. <https://doi.org/10.3390/coatings14050634>

Academic Editor: Xu Long

Received: 28 March 2024

Revised: 8 May 2024

Accepted: 16 May 2024

Published: 17 May 2024



Copyright: © 2024 by the authors. Licensee MDPI, Basel, Switzerland. This article is an open access article distributed under the terms and conditions of the Creative Commons Attribution (CC BY) license (<https://creativecommons.org/licenses/by/4.0/>).

1. Introduction

Nanoscience in physics and materials science primarily delves into understanding optoelectronics at nm-sized dimensions, while in chemistry, these applications are associated with several different systems, including but not limited to colloids, micelles, polymer composites, and other similar structures [1–9]. This overlapping of disciplines enables the engineering of novel materials with size-dependent optical properties, opening new avenues such as cybernetics, non-invasive clinical procedures, lab on a chip, and many environmental applications [9–19]. Semiconductor nanomaterials have attracted a lot of attention due to their widespread applicability in optoelectronics. Substantial efforts have been invested in the synthesis and characterization of semiconductor-based nanomaterials from groups II–VI, III–V, III–VI, and oxide-semiconductor materials until now [1]. Among these, a special class of materials are wide band gap II–VI semiconductors, since their bulk properties are within the visible spectrum and their applications have a wide range [1–3].

Quantum dots (QDs) are sometimes utilized in diverse and flexible applications across various environments, landscapes, and geometries [9,10]. Sometimes, using QDs directly in the application site can result in aggregation, potentially resulting in photodegradation [5,11]. One viable solution is the use of composite nanomaterials. Composite nanomaterials, which consist of more than one component, are employed in situations requiring flexibility and several of the properties coming from the components that are present. In many instances, QDs are dispersed within polymer matrices, forming a polymer nanocomposite (PN) [5,13]. In PN systems, the nanoparticles exhibit strong repulsion, thereby reducing the likelihood of aggregation [13]. PNs are particularly advantageous for designing novel materials due to their lightweight nature and ease of processing. Recent

theoretical calculations provide accurate predictions of the optical properties of PNs, offering a strong platform where predictive models enhance the optical properties of both the polymer and the QDs. The models include details of the chemical properties of the polymer matrices and the confinement-related properties of the nanoparticles [8–11].

Photoluminescence (PL) stands out as one of the most powerful fundamental properties of PN systems. Upon absorbing a suitable photon, an electron transitions into a higher energy state, before re-emitting another photon to relax back into the ground state [4]. The emitted photons typically possess lower energies or longer wavelengths because of Stoke's shift [4]. Although the basic mechanism remains the same, the specifics of the electronic transitions, metastable states, and relaxation processes are influenced by various factors, such as scattering, defect, or impurity states. The mechanism of detailed balance is also responsible in certain cases [2]. Therefore, characterizing photoluminescence (PL) from PNs becomes crucial, especially when they are in different chemical environments and/or subjected to varying interfacial interactions.

A wide range of applications, including but not limited to light-emitting devices, solar cells, sensors, nano-catalysts, greener memories, and engineering of tissues, has been achieved through II–VI PN materials [1,5–7,10,14]. CdSe PNs hold a special place among them and have been attractive for their suitability in synthesis recipes as a stable nanomaterial [14]. CdSe QDs typically consist of a CdSe core and a ligand shell. Ligands play crucial roles in maintaining the stability and solubility of the nanoparticles. Also, during the synthesis process, ligands play a stabilizing role by preventing the aggregation and precipitation of the nanocrystals, thus ensuring controlled growth. For all practical purposes, it is important to probe the effects of closely packed CdSe nanoparticles on their optical properties.

This work focuses on the synthesis of polymer materials doped with CdSe QDs exhibiting two distinct PL emission wavelengths. PL intensities from the two characteristic wavelengths, originating from QDs of different sizes within the system, were adjustable by varying the ratio of doped silica to polymethyl methacrylate (PMMA) microparticles. The objective of this study was to probe the effects of varying orange to red-emission peak intensity ratios on the PL emission intensities as the excitation intensity increases. The measurements captured the PL intensity growth when the laser excitation intensity was modified, by measuring the PL emitted from the two-colored QD systems. Examination of the data unveiled distinct trends in the growth of PL intensity concerning laser excitation when compared to similar CdSe PNs made with polyvinyl alcohol (PVA) matrix, as discussed herein [12]. The importance of this work could be noted: (a) in the uniqueness of the nanocomposite systems created and studied, (b) in the way their steady-state PL responds to the excitation intensity change, and (c) due to the link between the PL growth response to the relative amount of “red” dots present. Essentially, this report emphasizes the synthesis of a nanocomposite system that is easy to integrate and has unique optical limiting properties.

2. Materials and Methods

QD films with two nanoparticle sizes were generated by initially suspending the desired quantity of silica microparticles doped with “orange” QDs, which emit at around 578 nm, in 2.3 g of a 5% polymethyl methacrylate (PMMA) solution. To create a 50% silica film, 0.1 g of microparticles was incorporated, and for a 25% silica film, 0.04 g of microparticles was added, and so forth. A detailed description documented in an earlier report focused on PVA-based material, and hence only a brief overview will be included here [10,12]. First, the doping of silica microparticles with QDs was performed. This was achieved by creating a suspension of 0.1 g of commercially available silica microparticles (Sigma Aldrich, St. Louis, MO, USA) in 3 mL of stock solution of ammonia after mixing it with 4 mL of ethanol and 2 mL of distilled water. The mixture was stored in a 20 mL vial. Then, 10 mg of “orange” emitting quantum dots (QDs) were added to this solution before treating it with a surface ligand (3-Mercaptopropyl) trimethoxysilane (purchased from

Mesolight, Inc., Suzhou, China), with 0.4 g of tetraethyl orthosilicate (TEOS). At this point, the vial was sealed, before stirring the mixture for an hour at temperature. The reaction mixture was allowed to settle next. Once settled, the coloration of the supernatant was checked. In case there is a coloration, an extra amount (0.1 g) of TEOS is added, before repeating the stirring step for one more hour. The supernatant was made transparent by repeating the above two steps a few times. Next, 0.1 g of aminopropyltriethoxysilane (APTES) and 0.1 g of distilled water were added, and the reaction vessel was stirred for 2 h. The reaction product was centrifuged to gather the particles, before washing with isopropanol, and finally drying them under vacuum. After making a solution comprising microparticles and the polymer, careful mixing was carried out to achieve even dispersion. At this point, “red” QDs with PL at approximately 650 nm were added to the solution in instalments of 10 μ L and constantly mixed. After adding each instalment of “red” QDs, a droplet of the resulting product was checked under a microscope while being vacuum-dried. Throughout this text, the terms “orange” and “red” PL will occasionally be denoted as “peak 1” and “peak 2”, respectively. It is noteworthy that the difference in the fabrication process from one sample to another is only the relative amount (in volume) of the “red” (650 nm) vs. “orange” (578 nm) emitting QDs. Essentially, when “red” emitting QDs were added by volume in instalments of 10 μ L, after each instalment the relative PL intensities were checked. This process was stopped once the desired PL peak ratio was achieved.

Once the desired PL peak ratios were achieved, the solutions were drop-cast on 50.8 mm \times 50.8 mm \times 6.35 mm glass substrates (Chemglass Life Sciences LLC., Vineland, NJ, USA). The glass substrates were chosen based on their high transmittance in the wavelength range 300–2000 nm. During the drop cast process, \sim 5 μ L of the solution was pipetted on the glass substrate and the solution was spread using a spatula to have a uniform film. Once the films were dried, the drop cast samples were inspected using regular microscope (AmScope LLC., Irvine, CA, USA). Using surface profilometry (Dektak 3ST from Bruker Corporation, Billerica, MA, USA) the thicknesses of the films were found to be \sim 90 μ m with 5% or less variance. The PL peak position and intensity did not show any dependence on the thickness of the layer. Figure 1a illustrates a schematic cross-section of the sample, showing that the “orange” QDs are connected to silica, while the “red” QDs are evenly spread in the polymer matrix. The ratio was varied to probe the effect of the weak and strong presence on the interaction between the two QDs. The experimental setup is presented in Figure 1b. A closeup of the deposited PMMA1 film is shown in Figure 1c, showing reasonable smoothness on the surface. A scanning electron microscope (SEM) from Zeiss (White Plains, NY, USA) was used to comment on the texture and surface of the film, as could be seen in Figure 1d. The SEM confirmed the presence and uniformity of the deposited film. While no characterization of surface contamination could be made, it is safe to assume that the level of contamination has not impacted the overall PL signal, which is the focus of this study.

The comparative intensities from both PL peaks were investigated by exciting samples to a 405 nm diode laser with tunable power control. Table 1 outlines the 6 samples examined in this study, where PMMA1 refers to an “orange”：“red” intensity ratio of 10:1, PMMA2 refers to 8:1, and so on, as detailed in Table 1. The two PVA-based samples studied were PVA1 and PVA2, with the “orange”：“red” peak intensity ratios 4:1 and 2:1, respectively. The ratios were chosen (1) to probe the effects of the “orange”：“red” PL peak intensity ratio on the growth of PMMA-based samples, and (2) to compare PMMA and PVA-based samples with similar peak intensity ratios. PMMA3 and PVA1 share the same intensity ratio, and thus they are comparable for a preliminary investigation of the role of polymer in the PL properties. Similarly, PMMA4 and PVA2 are similar and hence have been compared in the discussion.

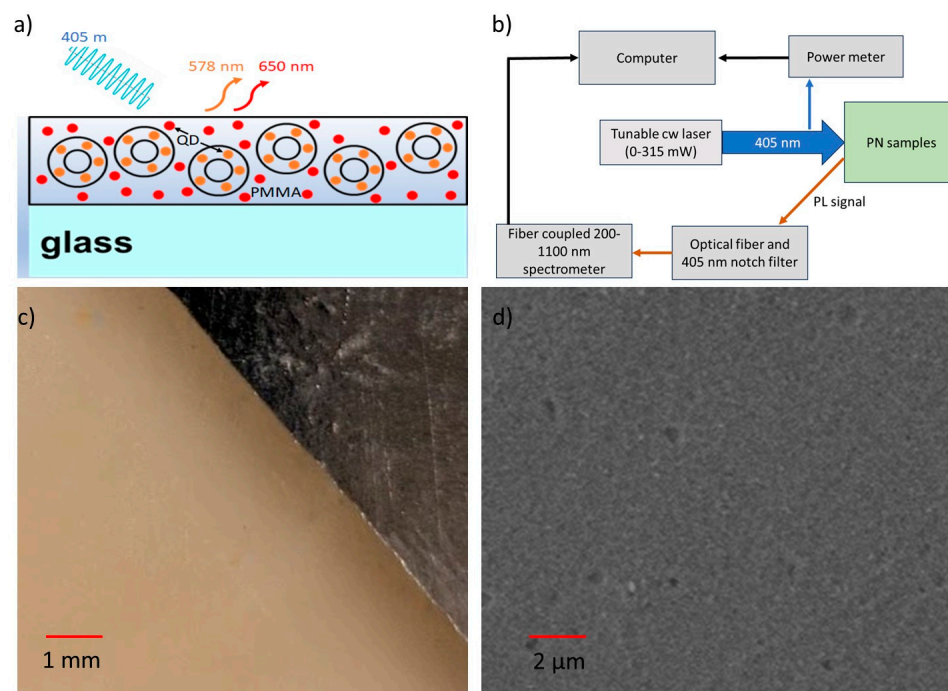


Figure 1. A schematic diagram of the cross-section of two-phase two-QD samples showing orange QDs bound in the shells of silica microparticles and “red” QDs dispersed in the surrounding polymer (PMMA) matrix (a). The “red” dots are representative of the 650 nm emitting QDs, whereas the “orange” dots are 578 nm emitting QDs encapsulated inside the silica microparticles (black concentric circles). The films were drop-cast on glass substrates. The experimental setup showing PL measurement scheme (b). A photograph of PMMA1 film deposited on glass, with an aluminum foil placed next to it for contrast (c), and an SEM image (d) of PMMA1 film.

Table 1. List of CdSe PNs synthesized and investigated.

Samples	Peak 1 and 2 Intensity Ratios at 405 nm, 0.014 W/cm ² Intensity
PMMA1	10:1
PMMA2	8:1
PMMA3	4:1
PMMA4	2:1
PVA1	4:1
PVA2	2:1

The PL was measured using a custom-built setup employing backscattering geometry, featuring a fiber-coupled spectrometer (Silver Nova from StellerNet Inc., Tampa, FL, USA). A schematic diagram is presented in Figure 1b. A 405 nm cw laser was used as the excitation source. The excitation laser intensities could be tuned through a calibrated average power vs. diode current curve, spanning from 0 to 315 mW with 3% or less fluctuations, monitored by a power meter from Laserglow Technologies (North York, ON, Canada). The laser powers were subsequently converted to intensities using the following formula:

$$\text{intensity (W/cm}^2\text{)} = \text{output power (W)}/\text{area of laser beam (cm}^2\text{)} \quad (1)$$

where, “output power” is defined as the measured power at the sample plane, while “Area” denotes the region covered by the laser beam at that plane. Unless specified otherwise, the exposure time was set at 5 s, and the beam area was estimated to be 0.1257 cm² for all reported measurements. PL was collected using a fiber-coupled assembly fitted with a 405 nm notch filter to separate the excitation signal from the PL. All experiments were

carried out at room temperature. Consequently, photoluminescence (PL) measurements were performed, varying the 405 nm laser intensity within the range of 0–2.5 W/cm².

All four samples were found to have stable and consistent PL at the respective peak wavelengths. A series of 10 measurements were made stretched over an interval of 1 minute confirming the stability and consistency of the samples, as presented in Figure 2a,b. It is clear from Figure 2a that the two peaks are reproducible and there is no significant variability in intensities for the 1-minute interval of time, which is much greater than the 5 s interval for which the samples were excited in the PL measurements in this work. In Figure 2b, the intensity and wavelength consistency are plotted vs. the number of “shots”. Each of the 10 measurements is referred to as “shots” in that plot. Albeit insignificant, the wavelength from peak 2 showed more variability (5% or less) relative to peak 1 (4% or less). All the PMMA-based samples reported here demonstrated similar consistencies. The PVA-based samples were also identical, as reported previously [12]. The measurements reported here have been repeated on multiple occasions on different days to ensure that the measurements are consistent, the changes in PL properties are reversible, and to rule out any degradation impacting the optical properties.

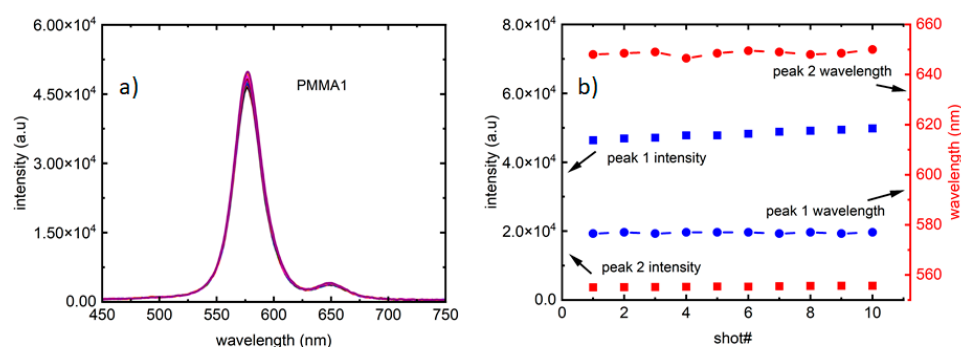


Figure 2. PL repeatability test for intensity and wavelength. (a) A total of 10 measurements (termed as “shots”) collected and overlaid for PMMA1, where different lines present the degree of fluctuations between shots within a period of 1 minute, which is 4% or less. (b) PL wavelength and intensity consistency for the two peaks for PMMA1 for the 10 shots.

3. Results

Once the initial characterization was complete, a systematic study of the PL growth was undertaken. Figure 3 presents the PL measurements from the four samples and the analysis. Figure 3a presents the four PMMA-based samples at a laser intensity of 0.2275 W/cm² excitation. The intensity ratios listed in Table 1 are for this excitation level. The ratios are dependent on not only individual peaks, but also their relative strengths, which is noteworthy, and not obvious from Figure 3a. The intensity growth in the PMMA-based samples seems to be sensitive to the presence of “red” quantum dots, emitting at 650 nm (also referred to as peak 2 in this work). Figure 3b–d present the growth of the two emission peaks as a function of laser excitation intensities. A comparison between the two peaks for PMMA1 is presented in Figure 3b as an example. While both peaks show similar trends in initial linear increase and eventual saturation, there are differences in thresholds of saturation, and the rapidity of intensity growth in them. This trend is seen in all PMMA samples, where the peaks grew almost linearly, after which a saturation of PL sets in. However, PMMA1 showed a larger saturation threshold for both peak 1 (~1.5 W/cm²) and peak 2 (~2 W/cm²), compared to other PMMA-based samples, where the saturation starts at ~1 W/cm². The intensities at which PMMA1 peaks saturated are also significantly higher than the other samples. For example, saturation level PL intensity in PMMA1 for peak 1 is ~4 times that of PMMA2 and PMMA3. Compared to PMMA4, PMMA1 is more than an order of magnitude higher in the saturating PL intensity for both peaks.

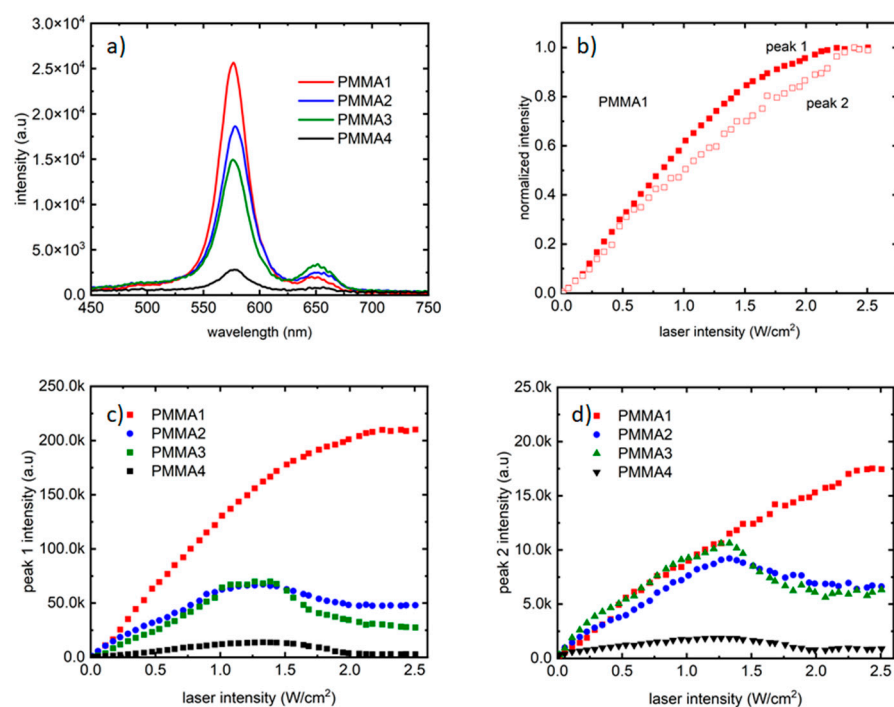


Figure 3. Fluorescence from the four samples as the excitation laser intensity varied from 0–2.5 W/cm². (a) The four PMMA-based samples studied, (b) evolution of PL peak 1 and 2 in PMMA1 with laser intensity, (c) PL peak 1 PL intensity growth in PMMA-based samples, (d) PL peak 2 PL intensity growth in PMMA-based samples.

Another important distinction is the presence of PL quenching in all PMMA-based samples except PMMA1. Figure 3c,d show clearly the reduction in peak intensities in PMMA2, PMMA3, and PMMA4, shortly after the saturation takes place. There is no quenching present in PMMA1. These features are unique, since in a previous report on PVA-based PN samples, there was no saturation reported for the 578 nm peak (or peak 1), while the 650 nm peak showed slight saturation at ~2.5 W/cm². This difference between PMMA-based and PVA-based PN can be seen readily in Figure 4, where the evolution of the two peaks was compared in two similar sets of samples. In Figure 4a, the 578 nm peak intensities are compared for two PMMA-based samples with two PVA-based samples. The peak intensity ratio in PMMA3 and PVA1 is 4:1, while the same for PMMA4 and PVA2 is 2:1. A similar comparison is presented for the 650 nm peak in Figure 4b. The difference in PMMA-based and PVA-based samples could be readily seen. Both PVA-based samples continued to grow linearly as a function of excitation intensity, and there is no trace of saturation for peak 1. The 650 nm peak (or peak 2) did saturate in PVA-based samples. However, the threshold of saturation is significantly lower in PMMA samples (~1 W/cm²) compared to the PVA samples (~2.5 W/cm²). Note that the general trend for PVA-based samples presented here is consistent with previous studies, irrespective of the peak intensity ratios [12].

Another aspect of the multiphase PL emissions is the peak shift as a function of laser excitation intensity. In a recent report, the PVA-based PNs have been found to emit at longer wavelengths at higher excitation intensities [12]. Figure 5 illustrates this through a comparison between PMMA and PVA-based samples, capturing the redshift for both peaks. Each symbol in Figure 5 presents an average of the peak positions found from all four samples, with the error bars showing standard deviation from them. There is hardly much difference in the redshifts of the two types of samples, except for slightly steeper shifts in PMMA-based samples, and an overall larger uncertainty, expressed as one standard deviation in the error bars.

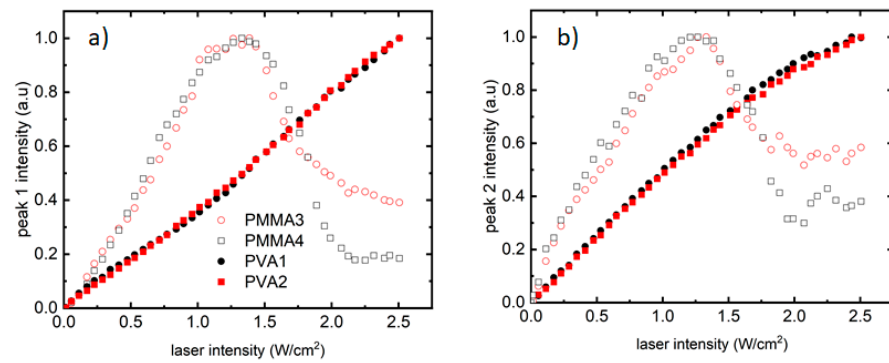


Figure 4. Comparison of the two PL peak intensity growths in PMMA-based (open symbols) and PVA-based (solid symbols) samples. (a) Comparison for the 578 nm peak and (b) the same for the 650 nm peak.

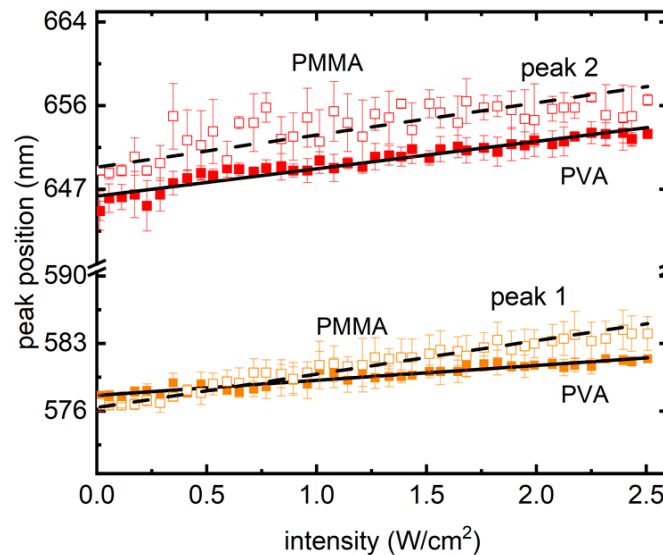


Figure 5. The shift in emission wavelength for the two peaks with increasing excitation intensity for PMMA (open symbols) and PVA (solid symbols)—based samples with similar peak intensity ratios where the error bars showing the standard deviation. The lines present linear fits to the peak positions for PMMA (dashed line) and PVA (solid line)—based materials.

A redshift in PL corresponds to a shrinkage of the band gap, which is different from single-phase QD films caused by dynamic band filling to increase the gap, resulting in a blueshift in PL peaks in those materials [11]. The linear redshift (goodness of fit > 96%) seen here is also different from previously reported nonlinear blueshift in PL peak wavelength, and has been modelled successfully using photo-dynamic Burstein–Moss theory [11].

4. Discussion

There are several major observations found in this study, such as: (1) a tunability in saturation intensities of both PL peaks, controlled by the relative peak intensity ratios, (2) dependence of PL-saturation on the amount of 650 nm QDs, (3) saturation and quenching in PMMA-based PNs, which was absent in PVA-based PNs, and (4) a redshift in both PL peaks as excitation intensity increased, a similar trait found in both types of PNs.

The tunability of saturation intensities, as shown in Figure 3c,d, is direct evidence that the 650 nm emitting QDs could control saturating PL intensities as well as corresponding excitation strengths needed. However, for “orange”：“red” ratios $\leq 8:1$, the samples also showed PL quenching when the excitation intensity grew higher. Saturation in QD systems has been reported previously and was attributed to the formation of a maximum number

of electron–hole (e–h) pairs possible to be created [2,7,12]. However, quenching was not seen in the previous studies. One of the most common contributors to any quenching mechanism in colloidal nanoparticle systems is Auger recombination, where a non-radiative energy dissipation contributes to the consumption of energy of the e–h pairs in radiative systems [19]. Hence, it is very likely that the different quenching in PL shown by the PMMA samples is a result of Auger recombination, which should be an efficient process in multi-carrier systems such as the ones being studied here. Auger recombination is a complex process, with multiple pathways possible for the systems to take depending on the core–shell geometries, the inter-particle distances, the dimensions of the dots and the surface states available in the systems [19].

It is very likely that a charge transfer mechanism is also contributing to the optical limiting behavior in the samples. This would explain the role of relative peak intensities on the overall saturation behavior. Clearly, when more 650 nm dots are available to participate in interdot optical exchange processes, more impact would be seen on the PL properties. Polymer-based multiple-sized CdSe QD systems were previously reported to have charge transfer processes present, resulting in quenching [20]. However, there was no prior evidence for quenching controlled by the choice of polymers. As shown in Figure 4, both QDs behaved differently when they were embedded in PMMA vs. PVA. The difference is most likely an attribute of nucleation in PVA resulting from water porosity which translates into changes in surface morphology and stiffness. It has been shown that PVA-based carbon dot PN system has differences in PL behavior because of the inherent properties of the polymer, that could be used to overcome the PL saturation in them [21]. This could explain the continuous growth in PVA-based PNs, vs. saturation and quenching in PMMA materials, which are not as porous, as seen in Figure 4. The morphology and surface roughness in PN systems significantly contribute to the optical properties. It is entirely possible that the surface morphologies of the two different polymers are partially responsible for the difference in optical losses, as was reported previously [22].

Both peaks almost linearly redshifted as the laser excitation intensity increased. However, PMMA-based samples showed larger sensitivity by shifting ~7 nm, compared to a marginal ~3 nm shift in PVA-based PNs at the highest laser excitation intensity of 2.5 W/cm². This is clearly a local stress-dependent property that is common in high-pressure PL properties [5]. Usually, compression allows the band gap to shrink in materials, making them emit at longer wavelengths, as seen to be happening in Figure 5. The red-shift could be quantified as a local stress metric, and hence the PNs could be utilized in pressure-sensing devices, as ultra-sensitive shock wave detectors.

The saturation and quenching behavior demonstrated by PN systems in this work could be classified as optical limiting, where the transmission of the material changes at higher laser intensity. This property could be employed in an all-optical switch. Unlike the PVA-based materials, where the PL peak intensities grow indefinitely and linearly, the saturation and subsequent quenching in PMMA-based materials make them extremely versatile with more than one, optically controllable PL peak intensity level.

5. Conclusions

The main purpose of this study is to highlight applications related to optical limiting properties in a PN system comprising CdSe and PMMA and to highlight the differences they have when compared to PVA-based similar systems. The PN system is easy to integrate, and partly linear and partly nonlinear behavior in its PL response when optical excitation is systematically increased.

All PMMA-based samples showed saturation. However, the saturation thresholds are different. PMMA1 saturated at ~1.5 W/cm² of laser intensity, while PMMA2 and PMMA3 saturated at ~1 W/cm². The two peaks, i.e., “orange” and “red” emission peaks evolved similarly with increasing laser excitation intensities. Interestingly, the PMMA-based samples showed photoinduced quenching as the excitation laser intensity reached 1.5 W/cm² and above, which was not present in the PVA-based samples of similar “orange”/“red” PL

peak intensity ratios. At $\sim 2 \text{ W/cm}^2$, the PMMA-based samples showed a second saturation of PL peak intensity, this time at a lower value. All photoinduced effects reported here are reversible, and the processes are nondestructive. PMMA-based samples showed better sensitivity to local stress compared to PVA-based samples by more than twice as much redshift.

A complete understanding of the mechanism in the evolution of PL in the four samples presented here seems complex and could be dependent on several factors. However, certain general observations could be made. The PMMA-based nanocomposites synthesized and characterized through PL here were found to be stable, consistent photoemitters with their peak 1 vs. peak 2 ratios staying the same for a large range of excitation intensities from a 405 nm laser. In contrast to previously reported PVA-based materials, the PMMA-based samples showed distinguishing saturation and quenching. The PNs showed consistent stress-dependent PL peaks, which are valuable as multiphase pressure-sensitive devices. The QD samples appear resilient to photo-induced permanent degradation which has been a critical issue in inorganic QD-based solar cells and light-emitting devices in the recent past [15–18]. Auger recombination and charge transfer could be the two major contributing factors in the observed PL saturation and quenching trends. The measurements reported here are exciting for future light-emitting device applications. The samples studied here use a simple recipe, making them a high-throughput synthesis process. Their PL intensity is substantial even in a thick film formation. They are easy to combine into different morphologies and shapes due to the inherent flexibility coming from the polymers.

Author Contributions: Conceptualization, M.B.; methodology, M.B.; formal analysis, M.B., L.M.E., J.F.R. and R.A.; investigation, L.M.E., M.B. and R.A.; resources, M.B.; data curation, M.B., J.F.R. and R.A.; writing—original draft preparation, M.B.; writing—review and editing, M.B.; supervision, M.B.; project administration, M.B. All authors have read and agreed to the published version of the manuscript.

Funding: This research received no external funding.

Institutional Review Board Statement: Not applicable.

Informed Consent Statement: Not applicable.

Data Availability Statement: The data presented in this study are available within the article.

Acknowledgments: M.B. thanks Bruno Ullrich for his valuable comments on the analysis.

Conflicts of Interest: The authors declare no conflict of interest.

References

1. Klimov, V.I. (Ed.) *Nanocrystal Quantum Dots*, 2nd ed.; CRC Press: New York, NY, USA, 2010.
2. Bhowmick, M.; Ullrich, B.; Murchland, M.; Zhou, X.; Ramkumar, C. Substrate and Excitation Intensity Dependence of Saturable Absorption in Perovskite Quantum Dot Films. *Nanomaterials* **2023**, *13*, 871. [CrossRef] [PubMed]
3. Moreels, I.; Kruschke, D.; Glas, P.; Tomm, J.W. The dielectric function of PbS quantum dots in a glass matrix. *Opt. Mater. Express* **2012**, *2*, 496. [CrossRef]
4. Ullrich, B.; Antillón, A.; Bhowmick, M.; Wang, J.S.; Xi, H. Atomic transition region at the cross-over between quantum dots to molecules. *Phys. Scr.* **2014**, *89*, 025801. [CrossRef]
5. Christensen, J.M.; Banishev, A.A.; Dlott, D.D. Bright emissive core-shell spherical microparticles for shock compression spectroscopy. *J. Appl. Phys.* **2014**, *116*, 033513. [CrossRef]
6. Kang, Z.; Banishev, A.A.; Lee, G.; Scripka, D.A.; Breidenich, J.; Xiao, P. Exploration of CdTe quantum dots as mesoscale pressure sensors via time-resolved shock-compression photoluminescent emission spectroscopy. *J. Appl. Phys.* **2016**, *120*, 043107. [CrossRef]
7. Bhowmick, M.; Singh, A.K.; Barik, P.; Xi, H.; Ullrich, B. All-optical switch based on PbS quantum dots. *Appl. Phys. Lett.* **2021**, *119*, 192103. [CrossRef]
8. Ullrich, B.; Xiao, X.Y.; Brown, G.J. Photoluminescence of PbS quantum dots on semi-insulating GaAs. *J. Appl. Phys.* **2010**, *108*, 013525. [CrossRef]
9. Zimnitsky, D.; Jiang, C.; Xu, J.; Lin, Z.; Tsukruk, V.V. Substrate- and Time-Dependent Photoluminescence of Quantum Dots Inside the Ultrathin Polymer LbL Film. *Langmuir* **2007**, *23*, 4509–4515. [CrossRef] [PubMed]
10. Christensen, J.M. Fast Photoemissive Probes for Shock Compression Microscopy. Ph.D. Dissertation, University of Illinois, Urbana, IL, USA, 2019. Available online: <http://hdl.handle.net/2142/104819> (accessed on 4 January 2024).

11. Ullrich, B.; Barik, P.; Singh, A.K.; García-Ramírez, E.V.; Reyes-Esqueda, J.A. Photo-dynamic Burstein-Moss doping of PbS quantum dots in solution by single and two-photon optical pumping. *Opt. Mater. Express* **2015**, *5*, 2431–2436. [[CrossRef](#)]
12. Bhowmick, M.; Christensen, J.; Adjorlolo, R.; Ullrich, B. Photoluminescence from two-phase nanocomposites embedded in polymers. *Micromachine* **2024**, *15*, 111. [[CrossRef](#)] [[PubMed](#)]
13. Hu, S.; Yan, X.; Zhang, Y.; Yang, B.; Li, H.; Sheng, C. Light-Induced Photoluminescence Quenching and Degradation in Quasi 2D Perovskites Film of $(\text{C}_6\text{H}_5\text{C}_2\text{H}_4\text{NH}_3)_2(\text{CH}_3\text{NH}_3)_2[\text{Pb}_3\text{I}_{10}]$. *Appl. Sci.* **2021**, *11*, 2683. [[CrossRef](#)]
14. Colvin, V.L.; Schlamp, M.C.; Alivisatos, A.P. Light-emitting diodes made from cadmium selenide nanocrystals and a semiconducting polymer. *Nature* **1994**, *370*, 354–357. [[CrossRef](#)]
15. Seitz, M.; Gant, P.; Castellanos-Gomez, A.; Prins, F. Long-Term Stabilization of Two-Dimensional Perovskites by Encapsulation with Hexagonal Boron Nitride. *Nanomaterials* **2019**, *9*, 1120. [[CrossRef](#)] [[PubMed](#)]
16. Khadka, D.B.; Shirai, Y.; Yanagida, M.; Miyano, K. Degradation of encapsulated perovskite solar cells driven by deep trap states and interfacial deterioration. *J. Mater. Chem. C* **2018**, *6*, 162–170. [[CrossRef](#)]
17. Li, R.; Yi, C.; Ge, R.; Zou, W.; Cheng, L.; Wang, N.; Wang, J.; Huang, W. Room-temperature electroluminescence from two-dimensional lead halide perovskites. *Appl. Phys. Lett.* **2016**, *109*, 151101. [[CrossRef](#)]
18. Yang, Y.; Yang, M.; Zhang, S.; Lin, X.; Dang, Z.; Wang, D. Photoinduced healing of polyolefin dielectrics enabled by surface plasmon resonance of gold nanoparticles. *J. Appl. Polym. Sci.* **2019**, *10*, 47158. [[CrossRef](#)]
19. Hou, X.; Kang, J.; Qin, H.; Chen, X.; Ma, J.; Zhou, J.; Chen, L.; Wang, L.; Wang, L.W.; Peng, X. Engineering Auger recombination in colloidal quantum dots via dielectric screening. *Nat. Commun.* **2019**, *10*, 1750. [[CrossRef](#)] [[PubMed](#)]
20. Kagan, C.R.; Murray, C.B.; Nirmal, M.; Bawendi, M.G. Electronic Energy Transfer in CdSe Quantum Dot Solids. *Phys. Rev. Lett.* **1996**, *76*, 1517. [[CrossRef](#)] [[PubMed](#)]
21. Elumalai, D.; Rodríguez, B.; Kovtun, G.; Hidalgo, P.; Méndez, B.; Kaleemulla, S.; Joshi, G.M.; Cuberes, M.T. Nanostructural Characterization of Luminescent Polyvinyl Alcohol/Graphene Quantum Dots Nanocomposite Films. *Nanomaterials* **2024**, *14*, 5. [[CrossRef](#)] [[PubMed](#)]
22. Baburin, A.S.; Moskalev, D.O.; Lotkov, E.S.; Sorokina, O.S.; Baklykov, D.A.; Avdeev, S.S.; Buzaverov, K.A.; Yankovskii, G.M.; Baryshev, A.V.; Ryzhikov, I.A.; et al. Evolutionary selection growth of silver films for low-loss nanophotonic devices. *Surf. Interfaces* **2023**, *39*, 102897. [[CrossRef](#)]

Disclaimer/Publisher’s Note: The statements, opinions and data contained in all publications are solely those of the individual author(s) and contributor(s) and not of MDPI and/or the editor(s). MDPI and/or the editor(s) disclaim responsibility for any injury to people or property resulting from any ideas, methods, instructions or products referred to in the content.